Intercalation

DOI: 10.1002/anie.200802598

Lattice Widening in Niobium-Doped TiO_2 Nanotubes: Efficient Ion Intercalation and Swift Electrochromic Contrast**

*Andrei Ghicov, Masahiro Yamamoto, and Patrik Schmuki**

The reversible intercalation of ions into and out of a host crystal lattice is the foundation of many applications, such as switchable electrochromic devices and rechargeable Li^+-ion batteries.[1–4] A frequently investigated host material is TiO_2, in rutile or anatase form, as the lattice allows small ions, such as H^+ or Li^+ ions, to be reversibly inserted from an electrolyte solution when a comparably low cathodic voltage is applied.[5] The insertion is accompanied by a reduction process, $TiO_2 + Y^+ + x\,e^- \leftrightarrow YTiO_2$ (Y^+ is the charged ion, for example, H^+ or Li^+). The formation of a Ti^{3+} species leads to a drastic change in the electronic and optical properties (a swift color change) of the material.[6–9] The kinetics and magnitude (color contrast) of H^+- or Li^+-ion insertion, as well as the reversibility of the electrochromic reaction, are controlled by solid-state diffusion/migration of the incorporated species. To shorten the solid-state diffusion path and time, efforts have been made to operate TiO_2-based devices with nanoparticulate systems.[10] Herein, we use a nanotubular geometry and show that the solid-state diffusion step can be drastically accelerated by a widening of the host TiO_2 lattice by niobium doping. Moreover, the lattice widening makes the TiO_2/Nb nanotubes much less sensitive to morphological damage in repeated intercalation cycles, compared with classical TiO_2 nanoparticles (such as Degussa P25) or undoped TiO_2 nanotubes. Furthermore, the lattice widening effected by niobium is so great that not only H^+ and Li^+ ions can be inserted into the widened TiO_2 lattice, but even much larger Na^+ ions.

Self-ordered nanotube layers can be grown using a simple electrochemical process on titanium and other transition metals.[11–16] The nanotube length can vary from approximately 100 nm to several hundred micrometers, and the diameter from 10 to 200 nm.[17,18] Generally, the "as-formed" nanotubes are amorphous, but they can be annealed to form a crystalline anatase structure.[19]

Figure 1b presents a layer (1 μm thickness) of TiO_2 nanotubes that were grown in a phosphate–fluoride electrolyte on a titanium substrate, and Figure 1c presents a layer (1 μm thickness) of TiO_2/Nb nanotubes that were grown under similar conditions on a β-$Ti_{55}Nb_{45}$ (β-Ti45Nb) substrate. For comparison, a film (1 μm thickness) of P25 nanoparticles on a titanium substrate is presented in Figure 1a. Compared

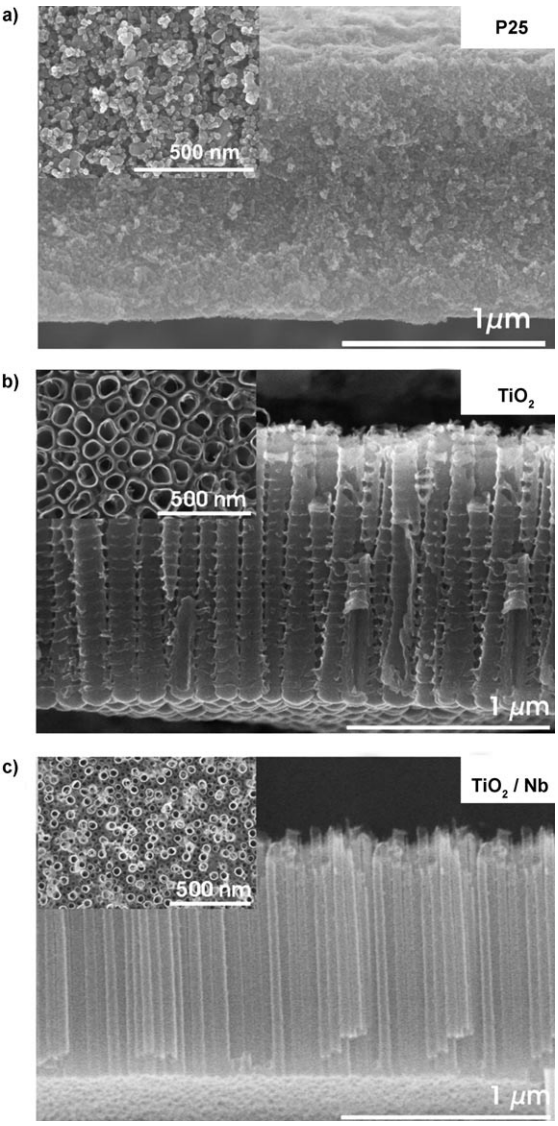

Figure 1. Field-emission scanning-electron microscope (FE-SEM) images of cross-sections and top views (insets) of a) a layer of P25 nanoparticles on a titanium substrate, b) a layer of TiO_2 nanotubes on a titanium substrate, and c) a layer of TiO_2/Nb nanotubes on a single-phase β-Ti45Nb substrate.

[*] A. Ghicov, Prof. Dr. P. Schmuki
University of Erlangen-Nuremberg
Department of Materials Science, WW4-LKO
Martensstrasse 7, 91058 Erlangen (Germany)
Fax: (+49) 9131-852-7582
E-mail: schmuki@ww.uni-erlangen.de
Prof. M. Yamamoto
Department of Energy and Hydrocarbon Chemistry,
Kyoto University, Nishikyo-ku, Kyoto 615-8510 (Japan)

[**] The authors acknowledge Sergiu P. Albu for XRD measurements, the DFG for financial support, and Robert P. Houser from ATI Wah Chang, an Allegheny Technologies Company, for providing the titanium–niobium alloy.

Supporting information for this article is available on the WWW under http://dx.doi.org/10.1002/anie.200802598.

to titanium or niobium substrates, titanium–niobium alloys provide greater geometrical flexibility with respect to the achievable tube length and diameter.[20] X-ray diffraction (XRD), energy-dispersive X-ray (EDX), and X-ray photoelectron spectroscopy (XPS) analyses showed that the as-formed TiO_2 and TiO_2/Nb nanotubes are amorphous, and that the TiO_2/Nb nanotubes have a uniform ratio of atomic concentrations (26% Ti, 13% Nb, and 61% O) over the entire length of the nanotubes.

For any intercalation application, the magnitude and speed of the intercalation process, the reversibility of the switching process, the required threshold potential for switching, and the long-term stability of the nanostructures are factors of prime importance. Figure 2 shows the coloration

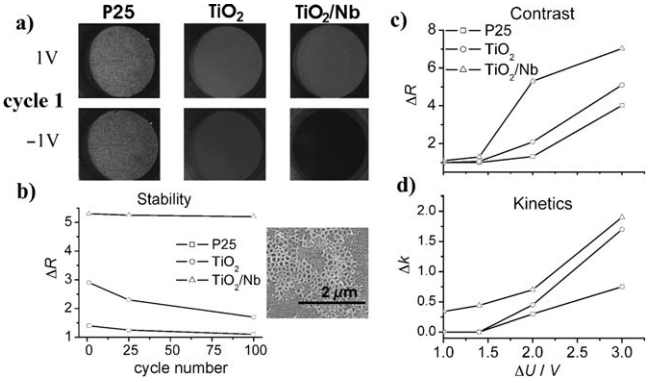

Figure 2. a) Photographs of the P25 nanoparticles, the TiO_2 nanotubes, and the TiO_2/Nb nanotubes polarized anodically at 1 V and cathodically at −1 V in 0.1 M $HClO_4$ (H^+ insertion) in the first cycle. b) Color contrast (ΔR) after 100 cycles of anodic/cathodic polarization (inset: SEM image of the TiO_2 nanotubes after 100 cycles). The anodic/cathodic potential was applied for 20 s. c) Color contrast and d) switching rate constant (Δk) calculated from reflectance measurements when a potential pulse was applied. $\Delta U = 1$ V corresponds to the potential switching from 0 to −0.5 to 0.5 V with a 20 s pulse.

and bleaching process for the three samples shown in Figure 1. Very strong color contrast is observed for the TiO_2/Nb nanotubes, while almost no color contrast is apparent for the P25 nanoparticles and the TiO_2 nanotubes (Figure 2a). The exchanged charges due to H^+ uptake and release are $Q_{P25} = 8.3\ mC\,cm^{-2}$ for the P25 nanoparticles, $Q_{Ti} = 76.4\ mC\,cm^{-2}$ for the TiO_2 nanotubes, and $Q_{TiNb} = 126.1\ mC\,cm^{-2}$ for the TiO_2/Nb nanotubes, indicating a significantly increased storage capacity in the niobium-doped nanotubes. Typical for intercalation processes with TiO_2 nanostructures is that repeated proton insertion and release leads to a slow, continuous deterioration of the nanostructures[21,22] (inset in Figure 2b) and a lower color contrast (ΔR). However, the TiO_2/Nb nanotubes retain their morphological integrity and color contrast during the entire cycling sequence (Figure 2b). The anodic charge after 100 cycles decreased by only 21% for the TiO_2/Nb nanotubes, while it dropped by a factor of two for the TiO_2 nanotubes and by a factor of three for the P25 nanoparticles.

From Figure 2c, it is apparent that a significantly smaller threshold potential for switching is required for the TiO_2/Nb nanotubes. For example, to achieve a color change of contrast comparable to that observed for the TiO_2/Nb nanotubes at ± 1 V ($\Delta U = 2$ V), switching potentials of ± 1.5 V ($\Delta U = 3$ V) and ± 2 V ($\Delta U = 4$ V) are necessary for the TiO_2 nanotubes and the P25 nanoparticles, respectively.

The insertion kinetics are significantly affected by the niobium doping of the TiO_2 nanotubes. From Figure 2d, it is apparent that the switching rate constants (Δk) determined for the TiO_2/Nb nanotubes are several times higher than for the other systems, particularly for moderate switching potentials. Even more drastic effects occur for the insertion of Li^+ ions and, surprisingly, Na^+ ions into the TiO_2/Nb nanotubes in non-aqueous electrolytes. While the insertion of H^+ and Li^+ ions into TiO_2 nanostructures is well-documented, there had not previously been a convincing demonstration that bigger ions, such as Na^+ ions, could be inserted into a TiO_2 nanostructure.

Figure 3 shows current-response and reflectance values for a series of different cathodic polarization potentials. For the three types of nanostructures, the insertion of Li^+ ions is

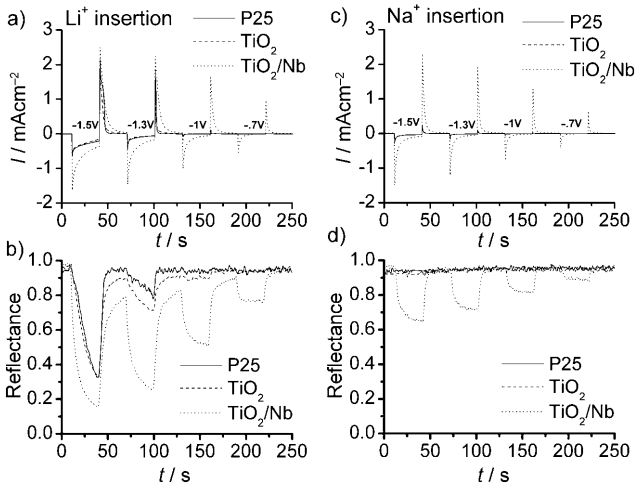

Figure 3. Amperometric measurements under different cathodic polarization potentials during potential pulsing in propylene carbonate containing a) 1 M $LiClO_4$ (Li^+ insertion) and c) 1 M $NaClO_4$ (Na^+ insertion) for the P25 nanoparticles, the TiO_2 nanotubes, and the TiO_2/Nb nanotubes. Reflectance measurements performed simultaneously with the amperometric measurements b) in (a) and d) in (c). The anodic potential used during potential pulsing was 0 V.

accompanied by a color change, once a threshold cathodic polarization potential is reached: for the P25 nanoparticles, the threshold potential is around −1.3 V, for the TiO_2 nanotubes it is around −1 V, and for the TiO_2/Nb nanotubes considerable switching occurs even at −0.7 V (Figure 3a and b). Under the experimental conditions used herein, no significant insertion of Na^+ ions was detected for the P25 nanoparticles or the TiO_2 nanotubes, whereas reversible insertion and release of Na^+ ions, combined with reversible

color switching, was detected for the TiO_2/Nb nanotubes (Figure 3c and d).

We ascribe the strong effects of the niobium doping of the TiO_2 nanotubes to a lattice expansion that widens the intercalation path for field-aided ion insertion and extraction.

Figure 4a shows the XRD patterns for the TiO_2 and TiO_2/Nb nanotubes annealed at 450 °C in air. Only anatase

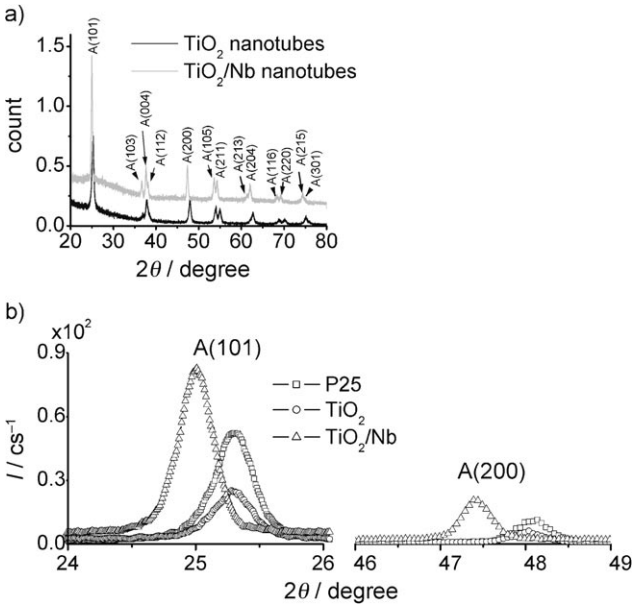

Figure 4. a) XRD patterns of the TiO_2 and TiO_2/Nb nanotubes after annealing at 450 °C for 1 h in air. Labels indicate anatase reflections. b) Comparison of the two main anatase peaks in the XRD patterns of the P25 nanoparticles, the TiO_2 nanotubes, and the TiO_2/Nb nanotubes.

reflections are detected in the XRD patterns of both types of nanotubes; no peaks that can be attributed to Nb_2O_5 or other niobium oxides are detected. However, for the TiO_2/Nb nanotubes, a shift of all the anatase peaks to lower θ values is observed in the XRD pattern (Figure 4b). By using Bragg's law,[23] assuming tetragonal symmetry, we calculated the following cell parameters: for the TiO_2 nanotubes, $a = 3.792$ and $c = 9.492$ Å, and for the TiO_2/Nb nanotubes, $a = 3.830$ and $c = 9.532$ Å (accuracy: ± 0.0005 Å).

Furthermore, the lattice expansion is supported by density functional theory (DFT) band calculations (see Figure S1 in the Supporting Information). The cell volumes and the c/a ratios of anatase (TiO_2) and of $NbTi_3O_8$ were obtained from total-energy calculations. In $NbTi_3O_8$, the central titanium atom of the Ti_4O_8 anatase unit cell is replaced by a niobium atom. The optimized volume of 143 Å^3 and the c/a ratio of 2.55 determined for anatase are in good agreement with the reported results.[24] The optimized volume of 146 Å^3 determined for $NbTi_3O_8$ (the optimized c/a ratio is 2.55) is greater than that for anatase. Moreover, the calculated energy barrier for the hopping of Li^+ ions between neighboring octahedral sites in anatase decreases by about 0.1 eV upon increasing the cell volume from 128 to 142 Å^3. The results are in line with the experimentally observed lattice widening and increasing of the switching rate constant in the TiO_2/Nb nanotubes, which lead to facilitated ion hopping (insertion) within the lattice.

In summary, the novel TiO_2/Nb nanotubes reported herein have a well-defined geometry, with a short diffusion length, and enlarged lattice parameters, which reduce the diffusion/migration barrier for small ions into the host structure. Therefore, the insertion of larger ions, such as Na^+ ions, is facilitated, uptake kinetics are greatly improved, storage capacity is increased, electrochromic color contrast is increased at a reduced switching potential, and resistance against electrode deterioration is increased.

Experimental Section

For the substrates, titanium (99.6% purity, Advent) and a single-phase β-Ti45Nb alloy (ATI Wah Chang) were cut into 2 × 2 cm pieces. These surfaces were polished using a suspension of 0.06 μm colloidal silica. Afterwards, the substrates were sonicated successively in acetone, isopropanol, and methanol, followed by rinsing with deionized water and drying in a nitrogen stream.

Details about the anodization set-up are given elsewhere.[25] To form the layers of nanotubes, the substrates were anodized in a phosphate–fluoride electrolyte (1 M NaH_2PO_4 + 0.5 wt % HF, pH 4.5) at 20 V (Ti) and 10 V (β-Ti45Nb). The potential was ramped from the open circuit potential (OCP) to the final potential with a step rate of 500 mV s^{-1} and was held at the final potential for 2 h. After anodization, the samples were rinsed with deionized water and dried in a nitrogen stream.

The film of P25 nanoparticles was prepared by dispersing P25 nanoparticles (0.5 g, Degussa) in deionized water (500 mL) and then ultrasonicating the dispersion for 30 min to obtain a uniform suspension. Afterwards, the suspension (1 mL) was applied to the mechanically polished metallic titanium surface and dried in air for several hours. The sample was then annealed for 1 h at 450 °C in air. The steps of applying the suspension to the titanium surface and thermally annealing the sample were repeated several times, until a thickness of approximately 1 μm was obtained.

Thermal treatments of the nanostructured layers were carried out using a rapid thermal annealer (Jipelec JetFirst 100) for 1 h at 450 °C in air, with a heating/cooling rate of 30 °C min^{-1}.

A field-emission scanning electron microscope (Hitachi FE-SEM S4800) was used for morphological characterization of the samples. The length of the nanotubes was directly obtained from SEM cross-sections.

XRD analysis was performed with a powder diffractometer (X'pert Philips PMD with a Panalytical X'celerator detector) using graphite-monochromatized $Cu_{K\alpha}$ radiation ($\lambda = 1.54056$ Å).

For the insertion of H^+, Li^+, and Na^+ ions, and for the electrochromic measurements, the samples were mounted into an O-ring-based electrochemical cell. Opposite to the sample, a platinum ring electrode and an Ag/AgCl electrode were used as counter and reference electrodes, respectively. The wall of the cell consisted of a quartz-glass window. The cyclic voltammetry and chronoamperometric measurements were performed using an Autolab/PGSTAT30 setup.

To evaluate the switching rate constant and the color contrast, reflectance measurements ($\lambda = 600$ nm) were carried out during potential pulsing in 0.1 M $HClO_4$ in water, in 1 M $LiClO_4$ in propylene carbonate, and in 1 M $NaClO_4$ in propylene carbonate. After the potential is switched to cathodic, the reflectance decreases exponentially according to $I = (I_{max} - I_{min})e^{-\Delta kx} + I_{min}$, where I_{max} is the maximum reflectance intensity, I_{min} is the minimum reflectance intensity, and Δk is the switching rate constant. The contrast of the color change is expressed by $\Delta R = I_{max}/I_{min}$.

Total-energy and force first-principles calculations were carried out using a plane-wave pseudopotential method in the framework of DFT.[26,27] We used Vanderbilt-type ultrasoft pseudopotentials[28] and the generalized gradient approximation (GGA) of Perdew–Wang for the exchange–correlation functionals.[29] A $20 \times 20 \times 8$ Monkhorst–Pack grid of special **k** points in the irreducible Brillouin zone and a plane-wave cutoff of 500 eV were used in the calculations. Activation energies were obtained from plots of energy versus lattice coordinates.

Received: June 3, 2008
Published online: September 9, 2008

Keywords: electrochromism · inorganic nanotubes · intercalation · lithium · sodium

[1] T. Ohzuku, T. Kodama, T. Hirai, *J. Power Sources* **1985**, *14*, 153 – 166.
[2] S. Y. Huang, L. Kavan, I. Exnar, M. Graetzel, *J. Electrochem. Soc.* **1995**, *142*, L142 – L144.
[3] T. Ohzuku, K. Sawai, T. Hirai, *J. Power Sources* **1987**, *19*, 287 – 299.
[4] C. R. Granqvist, *Nat. Mater.* **2006**, *5*, 89 – 90.
[5] M. Wagemaker, A. P. M. Kentgens, F. M. Mulder, *Nature* **2002**, *418*, 397 – 399.
[6] T. Ohzuko, T. Hirai, *Electrochim. Acta* **1982**, *27*, 1263 – 1266.
[7] M. P. Cantão, J. I. Cisneros, R. M. Torresi, *Thin Solid Films* **1995**, *259*, 70 – 74.
[8] B. Reichman, A. J. Bard, *J. Electrochem. Soc.* **1980**, *127*, 241 – 242.
[9] N. Özer, T. Barreto, T. Bueyueklimanli, C. M. Lampert, *Sol. Energy Mater. Sol. Cells* **1995**, *36*, 433 – 443.
[10] A. Hagfeldt, N. Vlachopoulos, M. Graetzel, *J. Electrochem. Soc.* **1994**, *141*, L82 – L84.
[11] V. Zwilling, E. Darque-Ceretti, A. Boutry-Forveille, D. David, M. Y. Perrin, M. Aucouturier, *Surf. Interface Anal.* **1999**, *27*, 629 – 637.
[12] R. Beranek, H. Hildebrand, P. Schmuki, *Electrochem. Solid-State Lett.* **2003**, *6*, B12 – B14.
[13] J. M. Macák, H. Tsuchiya, P. Schmuki, *Angew. Chem.* **2005**, *117*, 2136 – 2139; *Angew. Chem. Int. Ed.* **2005**, *44*, 2100 – 2102.
[14] J. M. Macak, H. Tsuchiya, L. Taveira, S. Aldabergerova, P. Schmuki, *Angew. Chem.* **2005**, *117*, 7629 – 7632; *Angew. Chem. Int. Ed.* **2005**, *44*, 7463 – 7465.
[15] H. Tsuchiya, J. M. Macak, I. Sieber, P. Schmuki, *Small* **2005**, *1*, 722 – 725.
[16] I. Sieber, H. Hildebrand, A. Friedrich, P. Schmuki, *Electrochem. Commun.* **2005**, *7*, 97 – 100.
[17] S. Bauer, S. Kleber, P. Schmuki, *Electrochem. Commun.* **2006**, *8*, 1321 – 1325.
[18] S. P. Albu, A. Ghicov, J. M. Macak, P. Schmuki, *Phys. Status Solidi RRL* **2007**, *1*, R65 – R67.
[19] R. Beranek, H. Tsuchiya, T. Sugishima, J. M. Macak, L. Taveira, S. Fujimoto, H. Kisch, P. Schmuki, *Appl. Phys. Lett.* **2005**, *87*, 243114.
[20] A. Ghicov, S. Aldabergenova, H. Tsuchiya, P. Schmuki, *Angew. Chem.* **2006**, *118*, 7150 – 7153; *Angew. Chem. Int. Ed.* **2006**, *45*, 6993 – 6996.
[21] R. M. Torresi, C. P. De Pauli, *Thin Solid Films* **1988**, *162*, 353 – 364.
[22] A. I. Shcherbakov, I. V. Kasatkina, *Prot. Met.* **2001**, *37*, 389 – 390.
[23] N. W. Ashcroft, N. D. Mermin, *Solid State Physics*, Holt, Rinehart and Winston, New York, **1976**.
[24] F. Tielens, M. Calatayud, A. Beltran, C. Minot, J. Andres, *J. Electroanal. Chem.* **2005**, *581*, 216 – 223.
[25] A. Ghicov, H. Tsuchiya, J. M. Macak, P. Schmuki, *Electrochem. Commun.* **2005**, *7*, 505 – 509.
[26] G. Kresse, J. Hafner, *Phys. Rev. B* **1993**, *47*, 558 – 561.
[27] G. Kresse, J. Furthmüller, *Phys. Rev. B* **1996**, *54*, 11169 – 11186.
[28] D. Vanderbilt, *Phys. Rev. B* **1990**, *41*, 7892 – 7895.
[29] J. P. Perdew, J. A. Chevary, S. H. Vosko, K. A. Jackson, M. R. Pederson, D. J. Singh, C. Fiolhais, *Phys. Rev. B* **1992**, *46*, 6671 – 6687.

